

All-optical quantum fluid spin beam splitterA. Askitopoulos,^{1,2,*} A. V. Nalitov,^{1,†} E. S. Sedov,^{1,3} L. Pickup,¹ E. D. Cherotchenko,¹ Z. Hatzopoulos,⁴
P. G. Savvidis,^{4,5,6} A. V. Kavokin,^{1,7} and P. G. Lagoudakis^{1,2}¹*School of Physics and Astronomy, University of Southampton, Southampton SO171BJ, United Kingdom*²*Skolkovo Institute of Science and Technology Novaya St., 100, Skolkovo 143025, Russian Federation*³*Department of Physics and Applied Mathematics, Vladimir State University named after A. G. and N. G. Stoletovs,
Gorky street 87, 600000 Vladimir, Russia*⁴*Microelectronics Research Group, IESL-FORTH, P.O. Box 1527, 71110 Heraklion, Crete, Greece*⁵*Department of Materials Science and Technology, University of Crete, 71003 Heraklion, Crete, Greece*⁶*ITMO University, St. Petersburg 197101, Russia*⁷*Spin Optics Laboratory, St. Petersburg State University, 1, Ulianovskaya, St. Petersburg 198504, Russia*

(Received 23 October 2017; revised manuscript received 14 December 2017; published 6 June 2018)

We investigate the spin behavior of the first excited state of a polariton condensate in an optical trap by means of polarization resolved spectroscopy. The interplay between the repulsive polariton interactions and the gain saturation results in a nontrivial spontaneous switching between the two quasidegenerate spatial modes of the polariton condensate. As a result, the polarization pattern of the emitted light dramatically changes. Successful harnessing of this effect can lead to a spin-demultiplexing device for polariton-based optical integrated circuits.

DOI: [10.1103/PhysRevB.97.235303](https://doi.org/10.1103/PhysRevB.97.235303)

Integratable spintronic devices are key elements for the implementation of spintronic circuits and spin-based quantum processors [1]. An important component of this architecture is a coherent spin beam splitter that can separate particles having different spins [2]. Since the first experimental demonstration of stimulated amplification and Bose-Einstein condensation (BEC) in semiconductor microcavities (MCs), polaritons have emerged as a promising platform for spintronic devices. They feature robust spin readout, long-range spin transport [3], electrical control of the condensate energy and spin [4–6], and room temperature operation [7]. Recent state-of-the-art MCs exhibit polariton lifetimes of hundreds of picoseconds and close to millimetre ballistic propagation lengths [8], while electrical creation of a polariton condensate has also been achieved [9]. Moreover, polaritonic systems have been shown to feature a wide range of resonant spin switching and multistability regimes [10,11], while the latest advances have also demonstrated spin switching and bistability in the nonresonant optical pumping configuration [12–14]. These advantages have lead to extensive theoretical suggestions of polariton-based spin circuits [15,16] as well as the realization of polariton optical spin filters [17]. However, a configuration that would allow for the directional and spatial separation of the spin components of a polariton condensate is yet to be demonstrated.

Coherent polariton circuits can be engineered by modifying the potential landscape of the microcavity through deep etching of the structure. In this way, a number of individual components of circuits have been realized such as polariton wires and routers [18,19]. Another approach is to modify the potential

landscape for polaritons by optical means through the strong excitonic interactions that dominate in the excitation region [20,21]. This method has the advantage of being actively tunable: different circuits can be created and tested on the same sample simply by modulating the spatial profile of the excitation [22]. This idea has led to the realization of different components of future all-optical polariton-based circuits such as all-optical polariton transistors [23] and amplifiers [24], while the hybridization of etching techniques and optical control has also been realized [25].

Although MC structures in the resonant excitation and optical parametric oscillator (OPO) regime have been proposed as the basis of spin-switching devices [10,11,26], the fine control of the excitation energy required for the switching operation hinders efficient applicability of these techniques. Nevertheless, optical control of the circular polarization of polariton emission has also been demonstrated under nonresonant optical injection in planar MCs [12,13,17,27,28], where intricate spin patterns have been observed due to the TE-TM splitting of the cavity mode [3,29,30].

In this paper, we study the first excited state of a polariton condensate in an annular optical trap. For a perfectly symmetric potential, we expect a twofold degeneracy of the first excited state (Ψ_{01}, Ψ_{10}), while for balanced population of the spin states the degeneracy is fourfold [Fig. 1(a)]. By introducing a small ellipticity in the spatial profile of the excitation, we lift the mode degeneracy (ΔE_l) of the trap and observe at threshold a p -orbital state. In this regime, we identify a density-dependent mode-switching behavior, where the coherent wave function spontaneously switches its orientation between two orthogonal axes. We allow for a small ellipticity in the polarization of the pump that lifts the spin degeneracy (ΔE_z) of the trap by inducing unequal spin populations. Examining the spin components of the condensate, we find that they switch

*Corresponding author: Alexis.Askitopoulos@soton.ac.uk

†Corresponding author: A.Nalitov@soton.ac.uk

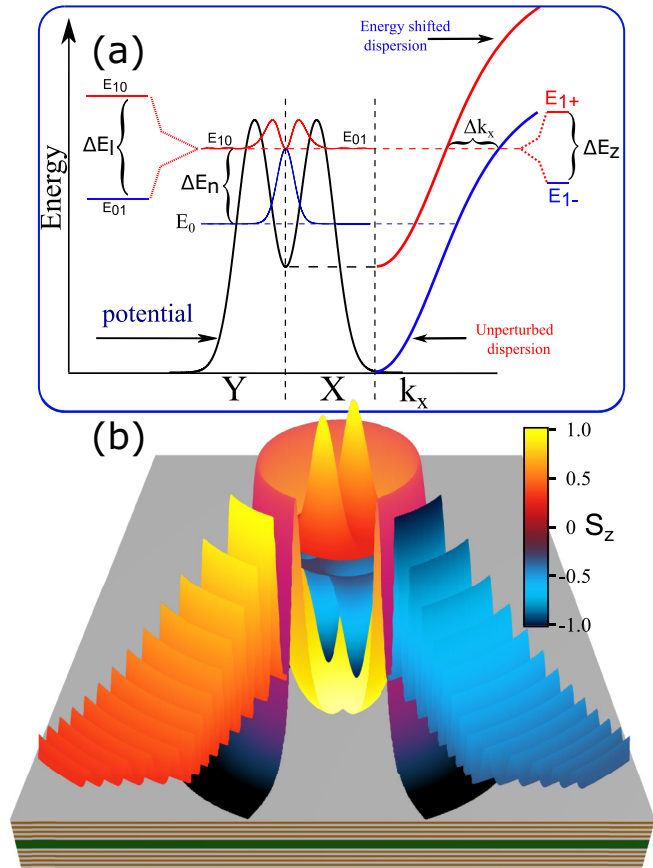


FIG. 1. Schematic representation of (a) the potential landscape of the system, detailing the fourfold degeneracy and (b) spinor polariton condensate wave functions and tunneling amplitudes in the trap.

independently and that, for a range of parameters, the two spinor condensates are oriented perpendicularly to each other giving rise to a butterfly spin pattern. We describe the system behavior within the framework of a two mode-Gross-Pitaevskii equation (GPE) model, where the two modes are coupled due to the spatially inhomogeneous depletion of the exciton reservoir and the repulsive exciton-polariton interaction. Polaritons can escape the finite trapping potential through resonant tunneling and are accelerated from the potential (by Δk_x). In the regime where the two spinor wave functions are oriented perpendicularly, the system spatially separates polaritons, escaping the trap based on their spin [Fig. 1(b)]. These results demonstrate that polariton condensates in optical traps offer unique possibilities for implementing spin logic and spin-demultiplexing operations in a solid state platform.

The structure we study here is a high quality ($Q = 16000$) $5\lambda/2$ GaAs microcavity with four triplets of 10 nm GaAs quantum wells and a Rabi splitting of ~ 9 meV. The sample is held in a cold finger continuous flow cryostat at ~ 6 K and is excited with a single mode, continuous wave (CW) Ti:Sapphire source that is tuned to the minimum of the photonic stop band at 754 nm. We use an acousto-optic modulator with a frequency of 5 KHz and a duty cycle of 1% to periodically switch off the CW optical excitation to avoid heating effects on the sample. We shape the spatial form of the excitation spot with the use of

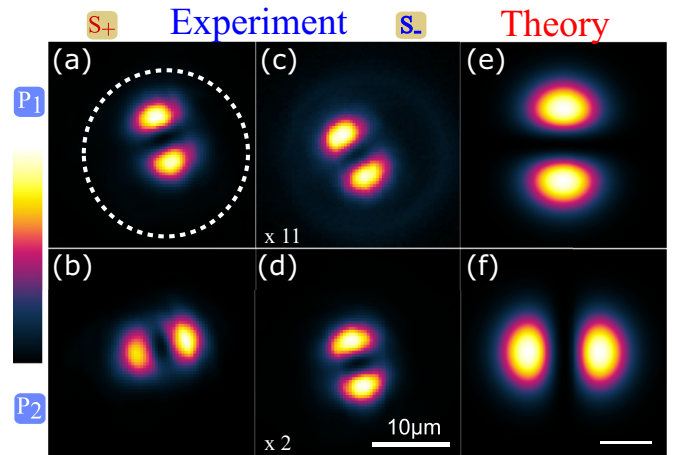


FIG. 2. Orientation switching of single spin component. Normalized intensity maps of (a),(b) S_+ spinor component for $P_1 = 1.2P_{th}$ and $P_2 = 1.4P_{th}$ and (c),(d) S_- spinor wave function. The white annulus in (a) outlines the excitation with the main axis of the ellipse along the vertical direction. (e)–(f) GPE simulation of a single component BEC for two densities above threshold, reproducing the switching operation. The scale bar of (e) and (f) is in dimensionless units of $\sqrt{2\beta/\alpha\Gamma}$.

a phase spatial light modulator in Fourier space and project the laser onto the sample with an optical system of two lenses and a high numerical aperture ($NA = 0.4$) objective. The sample was excited at a negative detuning of $\Delta = -5$ meV where the lower polariton mode has a calculated exciton Hopfield coefficient of $X_e = 0.25$, while the heavy hole exciton emission at 6K is at 1.456 eV. Photoluminescence emission from the sample is collected through the same objective, while a dichroic mirror filters out the optical excitation and with the use of a $\lambda/4$ wave-plate and a Wollaston prism, we simultaneously project both spin components of the signal to our imaging apparatus.

We shape the nonresonant excitation into an annulus with radius $r_{max} = 10.8 \mu m$ and a very small ellipticity ($\epsilon \sim 0.155$), while the full width at half maximum of the laser profile is $\sim 2.5 \mu m$. The annular excitation creates a nearly parabolic potential in the polariton energy landscape, effectively trapping polaritons and allowing condensation in the center of the potential for a given excitation density threshold ($P_{th} \approx 10.4 \pm 0.2$ mW). For these conditions, we observe that the dominant spinor state just above threshold ($P_1 = 1.2P_{th}$) has a p -orbital symmetry that is oriented along the main axis of the ellipse as shown in Fig. 2(a). Surprisingly, as we raise the excitation power slightly further ($P_2 = 1.4P_{th}$) we observe a switching of the orientation of the p orbital as shown in Fig. 2(b) by $\pi/2$. Here, the switching occurs between modes of the same order (Ψ_{01}, Ψ_{10}) with an energy splitting of the order of $\sim 10 \mu eV$, depending on the trap asymmetry, in contrast to switching between modes of different order where the energy spacing is significantly higher ($\Delta E_n \sim 50 \mu eV$) [31] and where the competition between modal gain and loss is enough to describe the transition [32,33]. Considering that the finite potential allows for polaritons to tunnel through the trap, this effect can in principle be used to seed and switch on subthreshold, optically or electrically created polariton states outside the optical trap, and thus perform routing operations [19,23].

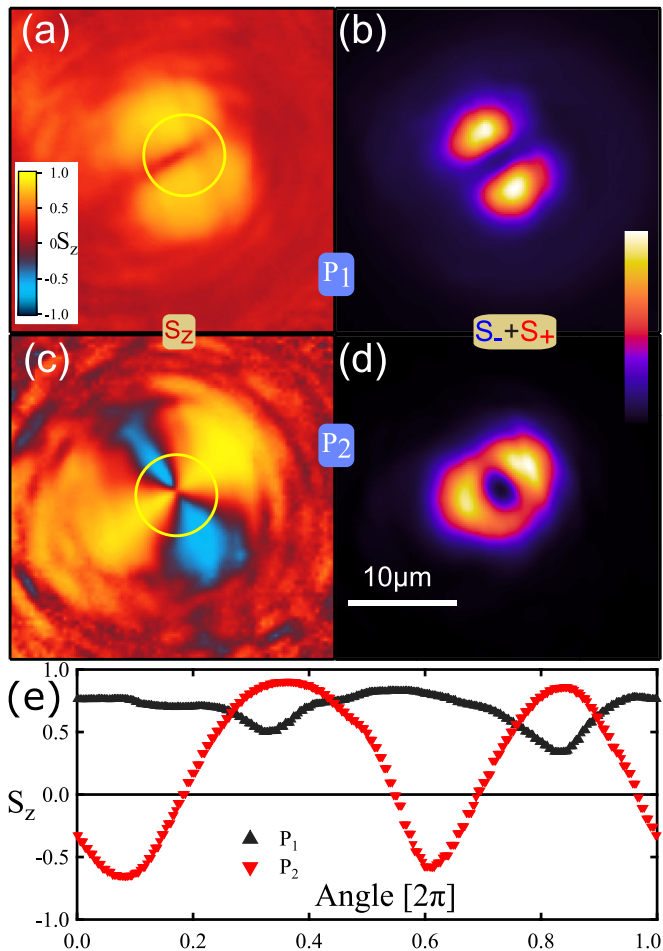


FIG. 3. False color scale spin textures and total intensity for aligned spinor wave functions at $P = P_1$ (a), (b) and for perpendicular spinor components at $P = P_2$, (c), (d) respectively. (e) S_z component for $r = 5 \mu\text{m}$ radius, outlined by the yellow circle in (a) and (c), plotted against azimuthal angle for P_1 (black triangles) and for P_2 (inverse red triangles).

Polariton condensates confined in parabolic optical traps demonstrate remarkable spin effects such as spin switching [12,13], spin bistability [14], and ferromagnetic phase transitions [12]. Polaritons have $+1$ and -1 spin projections to the growth axis of the MC that lead to right- and left-circular polarized photoluminescence. Resolving also the second spin component of the condensate, we note that at the onset of condensation, both are in the same configuration, though one component is populated more strongly ($\sim \times 11$), yielding a very high circular polarization of the emission of more than 80% [Figs. 2(a) and 2(c)]. As we increase the density to reach the switching threshold, we observe that when the dominant component switches its orientation [Fig. 2(b)], the low intensity spinor retains its initial configuration [Fig. 2(d)]. Nevertheless, as the two states are now primarily populated from different regions of the annular reservoir, the relative density ratio is reduced to only ~ 2.2 .

From the two spin images, we construct the real space map of the third Stokes parameter $S_z = (S_+ - S_-)/(S_+ + S_-)$, as well as the total intensity of the emission. In Figs. 3(a) and 3(b),

S_z and the total intensity are depicted for excitation power $P_1 = 1.2P_{th}$, showing the familiar spatial features of the Ψ_{01} trapped state. For $P_2 = 1.4P_{th}$, the spatial profile of S_z shows a spin precession around the core of the two orthogonally oriented components, whereas the total real space intensity distribution for this power resembles a doughnut or vortex state as expected from the linear superposition of the individual components, Figs. 3(c) and 3(d). In Fig. 3(e), the angular profile of the polarization map for the two excitation powers across the yellow circle of Figs. 3(a) and 3(c) is plotted, showing how the polarization profile of the collective mode changes from a nearly uniform angular distribution to an oscillating one.

Two-mode model. In the following, we neglect the coupling between the two polariton spin components, assuming weak effective spin-orbit interaction and weak interaction of polaritons with opposite spins. We also assume slow spin relaxation in the exciton reservoir on the timescale of its lifetime [34]. This allows us to treat each of the two decoupled spin components as an independent spinless condensate. In the mean field approximation, the latter is described by the wave function $\Psi(\mathbf{r}, t)$, which obeys the open-dissipative GPE [35]:

$$i \frac{\partial \Psi}{\partial t} = \left[-\frac{\nabla^2}{2m} + \frac{n}{2}(\alpha + i\beta) + \frac{\alpha_1}{2}|\Psi|^2 - i\frac{\Gamma}{2} \right] \Psi. \quad (1)$$

Here m is the effective mass, Γ is the inverse polariton lifetime, and $\hbar = 1$. The effective complex potential for polaritons depends linearly on the exciton reservoir density $n(\mathbf{r}, t)$. Its real part stems from the polariton repulsion by the reservoir, the strength of which is given by α . The imaginary part in turn describes stimulated scattering from the reservoir into the condensate, and is given by β . Finally, the repulsion strength of polaritons with the same spins is given by $\alpha_1 \approx X^2\alpha$, with X being the exciton Hopfield coefficient.

The GPE Eq. (1) is supplemented with the semiclassical equation on the exciton reservoir density:

$$\frac{\partial n}{\partial t} = P(\mathbf{r}) - (\beta|\Psi|^2 + \gamma)n, \quad (2)$$

where the gain term $P(\mathbf{r})$ is due to the inhomogeneous nonresonant optical pump and γ is the reservoir decay rate, while we neglect exciton mobility in the reservoir.

To describe the polariton eigenstates confined in the elliptic optical trap, we assume a paraboloidal form of the reservoir density $n(r, \varphi) = n(\varphi)r^2/R^2$, where R sets the size scale of the trap, and the angular density part

$$n(\varphi) = N_0 + n_0 + n_1 \cos(2\varphi) + n_2 \sin(2\varphi), \quad (3)$$

where N_0 is the reservoir density at the polariton lasing threshold, which is derived below, n_0 , n_1 , and n_2 are the angular harmonics of the reservoir density variation from N_0 . Alternatively, the angular dependent part of the exciton reservoir density may be introduced as

$$\delta n \cos(2(\varphi - \theta)) = n_1 \cos(2\varphi) + n_2 \sin(2\varphi), \quad (4)$$

with θ being the angle of the elliptic trap main axis.

In the linear regime, the polaritons are thus confined in a complex harmonic potential

$$U(r, \varphi) = \frac{m\omega_{\pm}^2}{2}r^2 \cos(\varphi - \theta)^2 + \frac{m\omega_{\pm}^2}{2}r^2 \sin(\varphi - \theta)^2, \quad (5)$$

characterized with complex frequencies

$$\omega_{\pm} = \sqrt{\frac{N_0\alpha}{mR^2}} \left(1 + \frac{i\beta}{2\alpha}\right) \left(1 + \frac{n_0 \pm \delta n}{2N_0}\right), \quad (6)$$

corresponding to the size quantization along the two main axes of the ellipse. Here we assumed the realistic case $\alpha \gg \beta$ for simplicity. The eigenstate energies

$$E_{i,j} = \sqrt{\frac{N_0\alpha}{mR^2}} \left(1 + \frac{i\beta}{2\alpha}\right) \times \left[\left(1 + \frac{n_0}{2N_0}\right)(1 + i + j) + \frac{\delta n}{2N_0}(i - j) \right], \quad (7)$$

are set by the two quantum numbers i, j , corresponding to size quantization along the elliptical axes. The wave functions, characterising the coherent polariton emission spatial profile, read

$$\Psi_{i,j} = \exp\left(-\frac{\xi_+^2 + \xi_-^2}{2}\right) H_i(\xi_+) H_j(\xi_-), \quad (8)$$

where $\xi_{\pm} = \sqrt{m\text{Re}\{\omega_{\pm}\}} r \cos(\varphi - \theta)$ and $\xi_{\pm} = \sqrt{m\text{Re}\{\omega_{\pm}\}} r \sin(\varphi - \theta)$ and $H_i(x)$ are the Hermite polynomials.

To account for polariton tunneling out of the trap potential, one may add the following orders into the harmonic potential. Phenomenologically, the tunneling rate may be accounted for in the state-specific decay rate $\Gamma_{i,j}$ of the quantum state. We address the experimentally relevant case where the maximum gain-loss difference $\text{Im}\{(1 + 2i)\omega_+ + (1 + 2j)\omega_-\} - \Gamma_{i,j}$ corresponds to the first excited doublet of states $i = 0, j = 1$, and $i = 1, j = 0$. In the following, we only keep the effective polariton decay rate $\Gamma = \Gamma_{0,1} = \Gamma_{1,0}$. The corresponding threshold reservoir density is then obtained by equating the polariton lasing gain term, given by the imaginary part of the confinement energy Eq. (7), to the loss term Γ :

$$N_0 = \alpha m \left(\frac{\Gamma R}{2\beta}\right)^2. \quad (9)$$

The doublet states Eq. (8) may be used to form a convenient basis of vortices, corresponding to a radially symmetric harmonic trap:

$$\Psi_{\pm}(r, \varphi) = \mathcal{A} r \exp\left(\pm i\varphi - m\Gamma \frac{\alpha r^2}{\beta 2}\right), \quad (10)$$

where \mathcal{A} is the normalization constant. Low ellipticity of the trap allows us to neglect both ground and the higher excited states and treat it as a small perturbation, coupling the two basis states, in the vicinity of the polariton lasing threshold. We thus project the GPE Eq. (1) onto the basis Eq. (10), putting $\Psi = \psi_+ \Psi_+ + \psi_- \Psi_-$. Excluding the optical frequency, we have in the rotating frame

$$i \frac{d\psi_{\pm}}{dt} = \frac{\Gamma}{2N_0} \left(\frac{\alpha}{\beta} + \frac{i}{2}\right) \left[n_0 \psi_{\pm} + \frac{\delta n}{2} e^{\mp 2i\theta} \psi_{\mp} \right] + \tilde{\alpha}_1 [|\psi_{\pm}|^2/2 + |\psi_{\mp}|^2] \psi_{\pm}, \quad (11)$$

where $\tilde{\alpha}_1 = \alpha_1 \int |\Psi_{\pm}|^4 d^2\mathbf{r}$. From Eq. (11), we derive the evolution of the condensate angular momentum $\mathbf{s} = \psi^\dagger \boldsymbol{\sigma} \psi$,

where $\psi = [\psi_+; \psi_-]$ and $\boldsymbol{\sigma}$ is the Pauli vector:

$$\frac{d\mathbf{s}}{dt} = \frac{\Gamma}{2N_0} \left[n_0 \mathbf{s} + \frac{1}{2} \mathbf{n} \mathbf{s} + \frac{\alpha}{\beta} [\mathbf{n} \times \mathbf{s}] \right] + \tilde{\alpha}_1 s_z [\mathbf{e}_z \times \mathbf{s}]. \quad (12)$$

Here $\mathbf{n} = n_1 \mathbf{e}_x + n_2 \mathbf{e}_y$ with $n_1 = \delta n \cos(2\theta)$, $n_2 = \delta n \sin(2\theta)$, and $\mathbf{e}_x, \mathbf{e}_y, \mathbf{e}_z$ are the unitary vectors along the principal axes of the system.

As the typical reservoir decay rate γ is much faster than the dynamics of the condensate, reservoir densities in Eq. (12) may be replaced with their equilibrium values, obtained from from Eq. (2) and linearized in s : $n_0 = (P - 2\tilde{\beta}s)/\gamma$, $n_1 = (\delta P - 2\tilde{\beta}s_x)/\gamma$, $n_2 = -2\tilde{\beta}s_y/\gamma$. Here P is the the angular independent part of the pumping power variation from the threshold $P_0 = \gamma N_0$, δP is its first angular harmonic and $\tilde{\beta} = \beta N_0 \int |\Psi_{\pm}|^4 d^2\mathbf{r}$. Equation (12) may be nondimensionalized by scaling energies in γ and densities in N_0 . Defining for convenience $\mathbf{S} = 2\tilde{\beta}\mathbf{s}$, $\tau = \Gamma t/2$, $\eta = \alpha/\beta$, and $\xi = \alpha_1/(\beta\Gamma)$, we arrive at

$$\begin{aligned} \frac{d\mathbf{S}}{d\tau} &= n_0 \mathbf{S} + \frac{1}{2} \mathbf{n} \mathbf{S} + [(\eta \mathbf{n} + \xi S_z \mathbf{e}_z) \times \mathbf{S}], \\ n_0 &= P - S, \quad n_1 = \delta P - S_x, \quad n_2 = -S_y. \end{aligned} \quad (13)$$

The first two terms in the right-hand part of Eq. (13) are the gain-loss part of the angular momentum evolution, while the third term describes its precession around an effective field, stemming from polariton repulsion from the reservoir and internal repulsion in the condensate.

We solve Eqs. (13) with the following parameters: $\eta = 10$, $\xi = 20$ $\delta P = 0.1$. There are two trivial stationary points of Eqs. (13), characterized with condensate populations $S^{\pm}(P) = \pm S_x^{\pm}(P) = (2P \pm \delta P)/3$. While the lower populated branch S_- is unstable, the other one is destabilized by the nonlinearities of Eqs. (13) above the critical pumping power $P_c = 0.2$ (corresponding to $1.2P_{\text{th}}$). At $P > P_c$, the only pair of stable stationary solutions $S(P)$ is symmetry breaking. Vorticity (S_z) sign in this phase is spontaneously chosen along with the sign of $S_y = -n_0 S_z / (\eta \delta P)$. The sign of S_x switches at the critical point, corresponding to the abrupt rotation of the condensate spatial density profile by $\pi/2$ at the switching power P_c . We also consider for comparison the purely photonic case $\xi = 0$ with no polariton repulsion. In the latter case, the switching occurs at $P = 0.1$ (corresponding to $1.1P_{\text{th}}$), the S_x component holds its value above the critical pumping and the condensate occupation $S^0 = P$ coincides with the asymptote of $S(P)$. The condensate population $S(P)$ is plotted in Fig. 4(a) along with the trivial branches $S^{\pm}(P)$, and the vectorial components of $\mathbf{S}(P)$ are shown in Fig. 4(b).

The spin patterns emerge in the case of elliptical pumping, where the pumping in two spin polarizations P^{\pm} are different. In the range of pumping powers where the predominantly pumped spin component of the condensate is in the broken symmetry phase $P^+ > P_c$, while $P^- < P_c$, the two spin components are spatially separated, resulting in the butterfly spin pattern. Spin patterns corresponding to different pumping power ranges are shown in Fig. 4(c). Note that artificial spatial noise is added in the regions where the condensate density is close to zero.

In conclusion, we have experimentally demonstrated and theoretically described a mode-switching process in a polariton

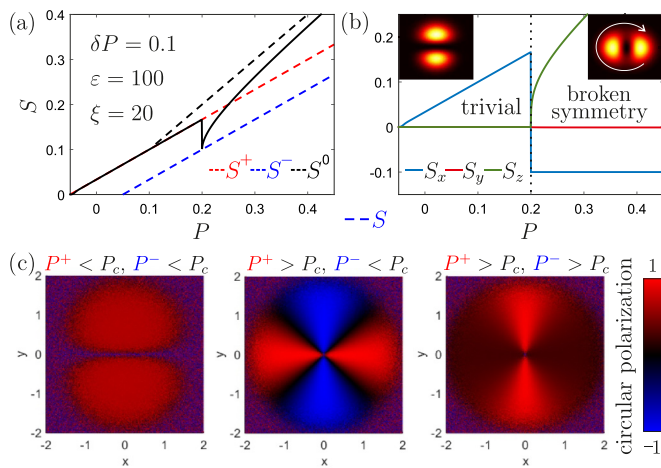


FIG. 4. The results of the spinless polariton condensate model, stable solutions of Eqs. (13). (a) Population versus pumping power. Mode switching occurs at $P_c = 0.2$. Trivial stationary branches S^\pm and nontrivial branch for the photonic case S^0 are plotted with dashed lines. (b) Angular momentum vectorial components. The spatial densities in the trivial and the broken symmetry phases are shown in the inset. (c) Circular polarization patterns in decoupled spin components model. Butterfly spin pattern emerges where one of the circularly polarized components is above threshold, while the pumping of the other component is below threshold, e.g., $P^+ > P_c$, while $P^- < P_c$.

optical trap, where the condensate wave function spontaneously changes its orientation with an adiabatic pump power increase. The effect is described by the nonhomogeneous depletion of the reservoir from different spatial modes coupled with the nonlinear interactions of the system. This configuration can, in principle, be exploited for the design and implementation of on-chip polaritonic routers and transistors. By means of polarization resolved experiments, we have shown that the two spin components of a polariton condensate can switch their orientation independently. Further examination of this system can lead to the development of an integrable all-optical spin beam splitter or spin demultiplexer. Furthermore, as polariton condensate lattices have now been proposed as an architecture for implementing quantum simulators [36] also in the trap configuration [37], these p -orbital states can be used for unidirectional coupling between neighboring nodes, increasing the complexity of the systems that can be studied.

This work was carried out in the framework of the joint Russian-Greek project ‘Polisimulator’ supported by the Ministry of Education and Science of The Russian Federation (Project No. RFMEFI61617X0085), Greece and the EU Regional Development Fund and the United Kingdom’s Engineering and Physical Sciences Research Council (Grant No. EP/M025330/1 on hybrid polaritonics). The data from this paper can be obtained from the University of Southampton ePrints research repository.

- [1] I. Žutić, J. Fabian, and S. Das Sarma, *Rev. Mod. Phys.* **76**, 323 (2004).
- [2] J. R. Petta, H. Lu, and A. C. Gossard, *Science* **327**, 669 (2010).
- [3] E. Kammann, T. C. H. Liew, H. Ohadi, P. Cilibrizzi, P. Tsotsis, Z. Hatzopoulos, P. G. Savvidis, A. V. Kavokin, and P. G. Lagoudakis, *Phys. Rev. Lett.* **109**, 036404 (2012).
- [4] G. Christmann, A. Askitopoulos, G. Deligeorgis, Z. Hatzopoulos, S. I. Tsintzos, P. G. Savvidis, and J. J. Baumberg, *Appl. Phys. Lett.* **98**, 081111 (2011).
- [5] P. Tsotsis, S. I. Tsintzos, G. Christmann, P. G. Lagoudakis, O. Kyriienko, I. A. Shelykh, J. J. Baumberg, A. V. Kavokin, Z. Hatzopoulos, P. S. Eldridge, and P. G. Savvidis, *Phys. Rev. Appl.* **2**, 014002 (2014).
- [6] A. Dreismann, H. Ohadi, Y. del Valle-Inclan Redondo, R. Balili, Y. G. Rubo, S. I. Tsintzos, G. Deligeorgis, Z. Hatzopoulos, P. G. Savvidis, and J. J. Baumberg, *Nat. Mater.* **15**, 1074 (2016).
- [7] S. Christopoulos, G. Baldassarri Hoger von Högersthal, A. Grundy, P. G. Lagoudakis, A. V. Kavokin, J. J. Baumberg, G. Christmann, R. Butté, E. Feltn, J.-F. Carlin, and N. Grandjean, *Phys. Rev. Lett.* **98**, 126405 (2007).
- [8] B. Nelsen, G. Liu, M. Steger, D. W. Snoke, R. Balili, K. West, and L. Pfeiffer, *Phys. Rev. X* **3**, 041015 (2013).
- [9] C. Schneider, A. Rahimi-Iman, N. Y. Kim, J. Fischer, I. G. Savenko, M. Amthor, M. Lerner, A. Wolf, L. Worschech, V. D. Kulakovskii, I. A. Shelykh, M. Kamp, S. Reitzenstein, A. Forchel, Y. Yamamoto, and S. Höfling, *Nature* **497**, 348 (2013).
- [10] A. Amo, T. C. H. Liew, C. Adrados, R. Houdré, E. Giacobino, A. V. Kavokin, and A. Bramati, *Nat. Photon.* **4**, 361 (2010).
- [11] T. K. Paraíso, M. Wouters, Y. Léger, F. Morier-Genoud, and B. Deveaud-Plédran, *Nat. Mater.* **9**, 655 (2010).
- [12] H. Ohadi, A. Dreismann, Y. G. Rubo, F. Pinsker, Y. del Valle-Inclan Redondo, S. I. Tsintzos, Z. Hatzopoulos, P. G. Savvidis, and J. J. Baumberg, *Phys. Rev. X* **5**, 031002 (2015).
- [13] A. Askitopoulos, K. Kalinin, T. C. H. Liew, P. Cilibrizzi, Z. Hatzopoulos, P. G. Savvidis, N. G. Berloff, and P. G. Lagoudakis, *Phys. Rev. B* **93**, 205307 (2016).
- [14] L. Pickup, K. Kalinin, A. Askitopoulos, Z. Hatzopoulos, P. G. Savvidis, N. G. Berloff, and P. G. Lagoudakis, *Phys. Rev. Lett.* **120**, 225301 (2018).
- [15] T. Espinosa-Ortega and T. C. H. Liew, *Phys. Rev. B* **87**, 195305 (2013).
- [16] T. C. H. Liew, A. V. Kavokin, and I. A. Shelykh, *Phys. Rev. Lett.* **101**, 016402 (2008).
- [17] T. Gao, C. Antón, T. C. H. Liew, M. D. Martín, Z. Hatzopoulos, L. Viña, P. S. Eldridge, and P. G. Savvidis, *Appl. Phys. Lett.* **107**, 011106 (2015).
- [18] E. Wertz, L. Ferrier, D. D. Solnyshkov, R. Johne, D. Sanvitto, A. Lemaître, I. Sagnes, R. Grousson, A. V. Kavokin, P. Senellart, G. Malpuech, and J. Bloch, *Nat. Phys.* **6**, 860 (2010).
- [19] F. Marsault, H. S. Nguyen, D. Tanese, A. Lemaître, E. Galopin, I. Sagnes, A. Amo, and J. Bloch, *Appl. Phys. Lett.* **107**, 201115 (2015).
- [20] G. Tosi, G. Christmann, N. G. Berloff, P. Tsotsis, T. Gao, Z. Hatzopoulos, P. G. Savvidis, and J. J. Baumberg, *Nat. Phys.* **8**, 190 (2012).
- [21] M. Aßmann, F. Veit, M. Bayer, A. Löffler, S. Höfling, M. Kamp, and A. Forchel, *Phys. Rev. B* **85**, 155320 (2012).
- [22] J. Schmutzler, P. Lewandowski, M. Aßmann, D. Niemietz, S. Schumacher, M. Kamp, C. Schneider, S. Höfling, and M. Bayer, *Phys. Rev. B* **91**, 195308 (2015).

- [23] D. Ballarini, M. D. Giorgi, E. Cancellieri, R. Houdré, E. Giacobino, R. Cingolani, A. Bramati, G. Gigli, and D. Sanvitto, *Nat. Commun.* **4**, 1778 (2013).
- [24] D. Niemietz, J. Schmutzler, P. Lewandowski, K. Winkler, M. Aßmann, S. Schumacher, S. Brodbeck, M. Kamp, C. Schneider, S. Höfling, and M. Bayer, *Phys. Rev. B* **93**, 235301 (2016).
- [25] C. Sturm, D. Tanese, H. S. Nguyen, H. Flayac, E. Galopin, A. Lemaître, I. Sagnes, D. Solnyshkov, A. Amo, G. Malpuech, and J. Bloch, *Nat. Commun.* **5**, 3278 (2014).
- [26] P. G. Lagoudakis, P. G. Savvidis, J. J. Baumberg, D. M. Whittaker, P. R. Eastham, M. S. Skolnick, and J. S. Roberts, *Phys. Rev. B* **65**, 161310 (2002).
- [27] M. D. Martín, G. Aichmayr, L. Viña, and R. André, *Phys. Rev. Lett.* **89**, 077402 (2002).
- [28] C. Antón, S. Morina, T. Gao, P. S. Eldridge, T. C. H. Liew, M. D. Martín, Z. Hatzopoulos, P. G. Savvidis, I. A. Shelykh, and L. Viña, *Phys. Rev. B* **91**, 075305 (2015).
- [29] P. Cilibrizzi, H. Sigurdsson, T. C. H. Liew, H. Ohadi, S. Wilkinson, A. Askitopoulos, I. A. Shelykh, and P. G. Lagoudakis, *Phys. Rev. B* **92**, 155308 (2015).
- [30] P. Cilibrizzi, H. Sigurdsson, T. C. H. Liew, H. Ohadi, A. Askitopoulos, S. Brodbeck, C. Schneider, I. A. Shelykh, S. Höfling, J. Ruostekoski, and P. Lagoudakis, *Phys. Rev. B* **94**, 045315 (2016).
- [31] A. Askitopoulos, T. C. H. Liew, H. Ohadi, Z. Hatzopoulos, P. G. Savvidis, and P. G. Lagoudakis, *Phys. Rev. B* **92**, 035305 (2015).
- [32] Y. Sun, Y. Yoon, S. Khan, L. Ge, L. N. Pfeiffer, K. West, H. E. Tureci, D. W. Snoke, and K. A. Nelson, *Phys. Rev. B* **97**, 045303 (2018).
- [33] L. Ge, A. Nersisyan, B. Oztop, and H. E. Tureci, [arXiv:1311.4847](https://arxiv.org/abs/1311.4847).
- [34] A. Vinattieri, J. Shah, T. C. Damen, D. S. Kim, L. N. Pfeiffer, M. Z. Maialle, and L. J. Sham, *Phys. Rev. B* **50**, 10868 (1994).
- [35] M. Wouters and I. Carusotto, *Phys. Rev. Lett.* **99**, 140402 (2007).
- [36] N. G. Berloff, M. Silva, K. Kalinin, A. Askitopoulos, J. D. Töpfer, P. Cilibrizzi, W. Langbein, and P. G. Lagoudakis, *Nat. Mater.* **16**, 1120 (2017).
- [37] H. Ohadi, A. J. Ramsay, H. Sigurdsson, Y. del Valle-Inclan Redondo, S. I. Tsintzos, Z. Hatzopoulos, T. C. H. Liew, I. A. Shelykh, Y. G. Rubo, P. G. Savvidis, and J. J. Baumberg, *Phys. Rev. Lett.* **119**, 067401 (2017).